Optimisation of a plasmonic parallel waveguide sensor based on amorphous silicon compounds

Costa, João, Fantoni, Alessandro, Lourenço, Paulo, Vieira, Manuela

João Costa, Alessandro Fantoni, Paulo Lourenço, Manuela Vieira, "Optimisation of a plasmonic parallel waveguide sensor based on amorphous silicon compounds," Proc. SPIE 11354, Optical Sensing and Detection VI, 113542K (13 April 2020); doi: 10.1117/12.2555842

SPIE.

Event: SPIE Photonics Europe, 2020, Online Only, France

Optimisation of a plasmonic parallel waveguide sensor based on amorphous silicon compounds

João Costa*[a,b], Alessandro Fantoni[a,b], Paulo Lourenço[b,c], Manuela Vieira[a,b,c]
[a] ISEL-Instituto Superior de Engenharia de Lisboa, Instituto Politécnico de Lisboa, Portugal
[b] CTS-UNINOVA, Caparica, Portugal
[c] DEE-FCT-UNL, Caparica, Portugal

ABSTRACT

This work reports the simulation of a plasmonic waveguide sensor working in the visible range based on amorphous silicon compounds. Typical plasmonic sensor interrogation schemes are based on scanning over the wavelength or the incident angle to search for the resonance condition. These solutions usually require expensive or bulky components, such as prisms, motor-driven rotation stages or tunable lasers. In this work we propose an amorphous silicon nitride waveguide structure consisting of an array of parallel surface plasmon interferometers of different lengths, each one comprising a thin layer of aluminium embedded into the waveguide. Using modal decomposition simulations, we show that the variation of the output power at the end of each waveguide array element provides a convenient interrogation scheme. By exploring amorphous silicon compounds that can be deposited by Pressure Enhanced Chemical Vapor Deposition (PECVD) at low temperatures, we aim to achieve a low-cost fabrication process that is compatible with back-end CMOS processing and wavelengths in the visible range.

Keywords: plasmonic sensor, waveguide, array, MMI, interferometer

*jcosta@deetc.isel.ipl.pt

INTRODUCTION

According to recent research trends[1], a key aspect for the advancement of the global healthcare system relies in the development of effective and affordable Point-Of-Care (POC) methods for medical screening and early diagnosis. In countries which face population aging such developments are driven by the need to continuously monitor the elderly and support positive aging strategies[2]. On the other hand, in places where the access to a hospital infrastructure is limited by large distances and economic reasons POC methods are critical to provide healthcare to the population. Lab-On-Chip (LOC) platforms are miniaturized analytical devices which integrate all functionalities on a single chip, from fluid handling, sample preparation (filtration, homogenization, and dilution), target detection, transducer readout, and signal processing. The development of a portable, easy-to-use and highly sensitive portable LOC platform for real-time diagnosis could offer significant advantages for future POC applications, entering in the daily routine of patients in a decentralized setting[3]. There are several efforts in progress[4], but few have reached the market[5]. The recent impressive acceleration of the consumer electronics technology opens a scenario for solving the problems related to miniaturization, multiplexing, automatization and network connectivity. The main point that remains critical is the sensing of biomarkers, often at extremely low concentrations and in the presence of other confounding molecules. This process is currently done in sophisticated, high-throughput laboratory machines and the challenge is to make it available in easy-to-use, portable devices for use by non-specialists in situ or for home operation[6].

From this point of view, the surface plasmon resonance (SPR) interferometric sensors can play a major role because they offer the potential of high sensitivity, a very high level of integration and relatively low fabrication complexity[7]. Still, in order for them to become widely used, materials and production techniques that are compatible with low-cost fabrication processes are necessary. Thin film semiconductors deposited by Pressure Enhanced Chemical Vapor Deposition (PECVD) have the potential to fulfil this requirement and are also compatible with standard back-end CMOS processing and integration[8]. The high refractive index of refraction of a semiconductor material allows a high level of integration but poses difficulties in the excitation of the surface plasmon polaritons. Although it is possible to use the *Kretschmann* configuration, such approach is not very suitable to be used in a small portable device. One alternative is using the

Optical Sensing and Detection VI, edited by Francis Berghmans, Anna G. Mignani, Proc. of SPIE
Vol. 11354, 113542K · © 2020 SPIE · CCC code: 0277-786X/20/$21 · doi: 10.1117/12.2555842

interferometric structure proposed by P. Debackere et al. [9], where the sensing mechanism is based on measuring the interference between two surface plasmon polaritons generated on the two surfaces of the metal layer.

Silicon is the most used semiconductor for photonic Integrated circuits (PIC). One major reason for the choice of silicon is the possibility of preparing integrated photonic and electronics structures compatible with the standard CMOS technology. Silicon is also the first-choice material for biosensors based on waveguiding structures, lab-on-chip platforms and point-of-care devices[10]. The absorption properties of silicon exclude the possibility of working in the visible range, silicon waveguides cover a wavelength spectrum starting at 1100nm, where most of the results target the telecommunication windows of 1550 and 1310 nm. Silicon Nitrate (SiN) has been recently proposed[11] as a PIC alternative technology, with a transparency window extended to the visible wavelength range, starting at 400 nm. SiN waveguides with SiO_2 cladding maintain a good refractive index contrast, allowing banding radius at the micrometric scale. Standard deposition method for SiN used in most of the foundries offering generic PIC fabrication is low-pressure chemical vapor deposition (LPCVD) [12]. SiN produced by LPCVD presents a high purity and homogeneity, but it is deposited at high temperatures (about 700 °C), making it not usable for integration with other materials which cannot withstand exposition to such high temperatures, as for example plastics substrates for flexible devices[13]. On the other hand, the plasma-enhanced chemical vapor deposition (PECVD) technique can be used to deposit thin film semiconductors and good quality SiN, at low temperatures between 200 and 400 ºC, providing a very attractive route towards high-volume fabrication of integrated photonic devices[14]. Amorphous silicon compounds produced by PECVD, like a-SiC:H, a-SiN:H or a-SiCN:H, are very attractive for the realization of low-cost photonic circuits. Also, the control of the compound percentages, hydrogen concentration and deposition conditions allows the fine tuning of the material structural and optical properties, including the possibility to work under different light wavelengths, opening the possibility to operate in the visible range of the spectrum[15]. The PECVD process also allows further integration with additional nanomaterials or nanostructures for improving the SPR effect for biosensing applications[16].

We have used in our simulations an amorphous silicon nitride (a-SiN:H) waveguide interferometric structure with an aluminium metal layer, working at 633 nm (He-Ne Laser beam). A novel interrogation scheme is proposed to overcome the complexity due to the traditional scanning over the wavelength or the incident angle, which inhibits the integration of the system into a fully on-chip solution. We have proposed an integrated system which consists of a Multi-Mode Interference (MMI) device working as a splitter to excite and an array of interferometers with different lengths. The variation of the output intensity at the end of each array element provides a convenient interrogation scheme which is dependent on the refractive index of the sample medium[17].

THEORY AND METHODS

Surface plasmon polaritons (SPP) are electromagnetic excitations propagating at the interface between a dielectric and a conductor, confined in the perpendicular direction. Under specific conditions, the evanescent waves became coupled to the surface collective oscillations of the free electrons, supporting their propagation at the metal-dielectric interfaces. In a simplified manner, it is possible to consider SPPs as hybrid modes comprising the features of both the propagating EM waves, and free electron plasma oscillations in metals, which are longitudinal. The TE waves cannot be coupled to the longitudinal electron oscillations in metals, only TM modes can couple to SPPs waves. The mode propagation constant β_{SPP} is given by[18] :

$$\beta_{SPP} = \frac{\omega}{c}\sqrt{\frac{\varepsilon_m(\omega)\varepsilon_d(\omega)}{\varepsilon_m(\omega)+\varepsilon_d(\omega)}} \quad (1)$$

where ε_m is the complex permittivity of the metal, ε_d the permittivity of the dielectric, ω the angular frequency and c the velocity of light. The mode propagation constant β_{SPP} is a complex number and the excitation of a SPP requires the existence of a positive real part. Such necessary condition is verified in a large variety of metal/dielectric combinations in the visible and in the infrared range. The imaginary part of β_{SPP} determines the attenuation of the SPP, and for relatively large values, practical applications are not viable. To study the conditions for SPP excitation, we have used the refractive index values of aluminium from Rakić et al.[19] and for amorphous silicon nitride the values reported in the literature[20] for a deposition temperature of 300ºC.

The schematic of the setup is presented in Figure 1. In order to excite the parallel waveguides a Multi-Mode Interference (MMI) device is used in a 1-to-N splitter operation mode[21]. Such operation mode can be achieved by centre feeding the MMI with a symmetric field profile and adjusting the length of the device, L_{MMI}, to the exact distance where the N-fold images are generated[22]:

$$L_{MMI} = \frac{n \cdot W_{MMI}^2}{N \cdot \lambda_0} \quad (2)$$

where λ_0 is the free space wavelength, W_{MMI} is the width of the device in the direction transversal to propagation and *n* is the real part of the refraction index of the material. The images are symmetrically located along the transversal direction with equal spacings W_{MMI}/N.

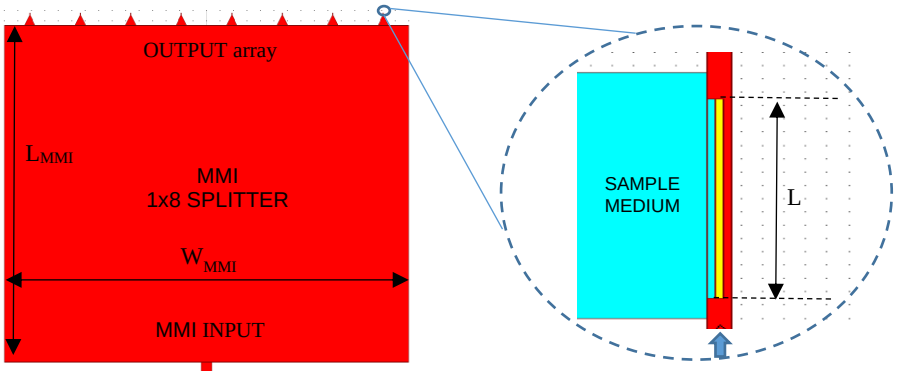

Figure 1. Schematic setup of the proposed structure. The a-SiN:H is represented in red, the aluminium film in yellow, the sample medium in cyan. The waveguide cladding (white background) is silicon dioxide. A zoom of the interferometer region is highlighted in the circle.

Figure 1 displays the interferometer and sample medium. The aluminium film (thickness 40 nm) is positioned at the centre of the waveguide (thickness 220 nm). The operation wavelength was set to λ_0=633 nm. Two SPPs are formed in the aluminium film, one on the left interface, which is identified with propagation constant $\beta 1_{SPP}$, and the other on the right interface, with propagation constant $\beta 2_{SPP}$. Since the two SPPs in general have different propagation constants their phase difference at the end of the plasmonic section will be a function of L:

$$\Delta\phi = (\beta 2_{SSP} - \beta 1_{SSP})L \quad (3)$$

When the SPP modes terminate in phase, constructive interference occurs and transmission of power to the output is maximal. On the contrary, out of phase SPPs will generate destructive interference and reduce the output guided power[9]. Since $\beta 1_{SPP}$ is dependent on optical properties of the sampling medium, changing the analyte concentration will have impact on the output power. The array of waveguides of different L provides the interrogation scheme.

The propagation of light is simulated using the mode expansion and propagation method. In this method, the waveguide is divided into longitudinally uniform sections and, in each section, the eigenmodes are calculated. Based on boundary conditions the modal amplitudes at both sides of the interface between the longitudinal sections are obtained. For this purpose, we have used the software package *modeprop* (Rsoft, Synopsys Inc.).

RESULTS AND DISCUSSION

The SPP propagation constant calculated from eq. (1) assumes a semi-infinite geometry which is a reasonable approximation for the sampling medium interface, but not for the opposite side where the SPP evanescent field is expected to extend to the cladding region. To take in consideration the cladding the propagation modes were obtained using the Finite Element Method (FEM) as implemented in the software package *femsim* (Rsoft, Synopsys Inc.). Figure 2 displays the SPP Hy field and propagation constants ($\beta = n_{eff}\ 2\pi / \lambda_0$) where we have assumed the sample medium is water.

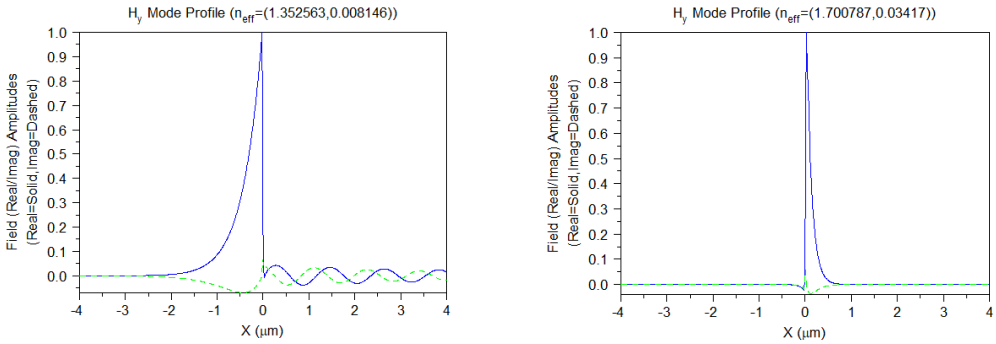

(a) (b)

Figure 2. Hy field of the SPP travelling in the interface (a) aluminium-water and (b) aluminium - a-SiN:H

Based on the propagation constants, $\beta 1_{SPP}$ and $\beta 2_{SPP}$, obtained we have simulated the interferometers in the constructive and destructive condition: $L = p\,\pi / (\beta 2_{SPP} - \beta 1_{SPP})$ where p is odd for destructive interference and even for constructive interference. We present the results in Figure 3 for p=1 and p=2.

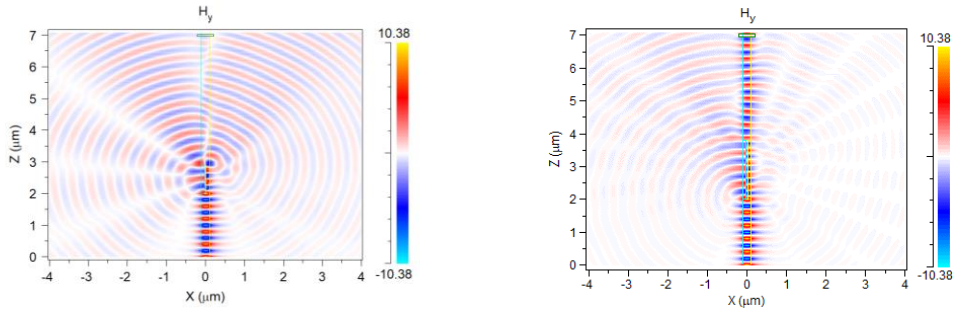

(a) (b)

Figure 3. The Hy field for the waveguide and interferometer region. The length of the interferometer L was adjusted for (a) destructive interference and (b) constructive interference.

In Figure 3(a) the destructive interference is clearly seen with the SPPs arriving at the end of the aluminium film in phase opposition. On the contrary, in subfigure (b) the SPPs arrive in phase and the field strength at the output increases significantly. In order to better visualize the relation between L and the power transmitted, simulations were performed, and the results are presented in Figure 4. The simulation results agree with the expected periodicity for in phase and out of phase lengths with the first minimum for L just below 1 μm and the first maximum close to 2 μm. We also present in the same figure the influence of the metal film thickness on the output response. It becomes clear that reducing the metal film thickness in the range 100nm to 40nm makes the difference between maximums and minimums more pronounced which is an advantage in terms of sensitivity. We have assumed a 40 nm thick metal film in the following simulations. In principle the thickness could be further reduced however this was not pursued to avoid imposing hard constraints on the fabrication process.

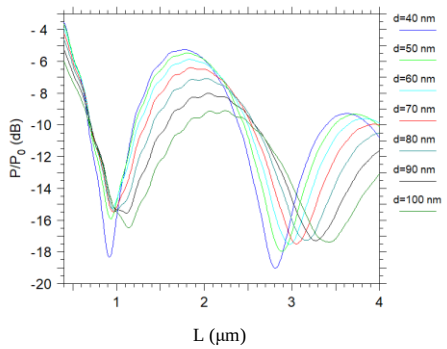

Figure 4. Fraction of the transmitted power as a function of the length of the interferometer (L) and the thickness of the Al layer (d)

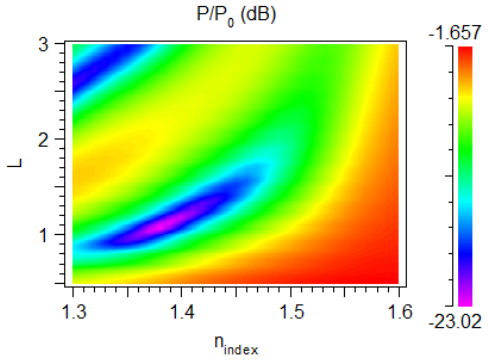

Figure 5. Fraction of the transmitted power as a function of the length of the interferometer and sample medium index

In Figure 5 the transmitted power is displayed as a function of the refractive index of the sampling medium and the length L of the interferometer. As the refractive index of the sampling medium increases the length periodicity also increases. This is expected since the SSP plasmons become more similar on both sides of the interface and therefore phase shifting requires larger distances.

The width of the MMI must be large enough to minimize interference between array elements. We have designed a 1x8 splitter with W_{MMI}=60μm and calculated L_{MMI} from eq. (2). The electric field strength at the output of the MMI structure is presented in Figure 6 where we can see that 8 peaks are generated at the output waveguide positions, as expected.

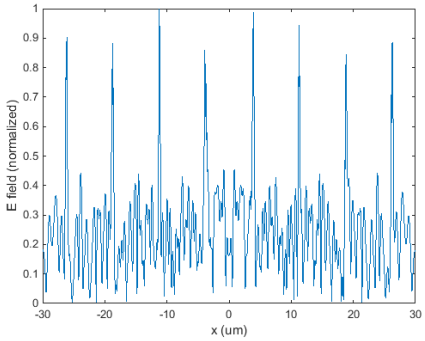

Figure 6. Electric field strength at the end of the MMI device.

Finally, the complete structure was simulated. The array elements were designed with interferometer lengths L=0.5+0.25*i μm, where i is the waveguide number, 1 to 8. We can observe in Figure 7 the transmitted power for each waveguide using four different refraction indexes n of the sampling medium. We can see that the minimum transmitted

power shifts from the 2nd to the 8th waveguide as the refractive index increases from 1.3 to 1.5. In fact, as the refractive index increases the minimum shifts to elements to the right which have longer L in agreement with the behaviour of the isolated interferometer.

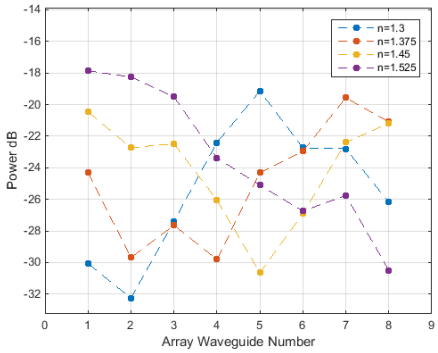

Figure 7. The output power of the array is dependent on the refraction index of the sample medium.

The results show that is possible to use the arrayed structure of interferometers in the visible wavelength as a direct interrogation scheme for retrieving information about variations of the refractive index of the sample medium. The refractive index is directly related to the position of the minimum output power in the array. Further optimization of the length of the MMI could be performed to achieve a more levelled power distribution at the input of each array element minimizing the influence of the non-ideal behaviour of the MMI.

This innovative approach eliminates the building complexity associated with mechanical and optical setups, targeting directly the lab-on-chip paradigm for Point-of-Care applications. Furthermore, as the result relies on the relative output power of elements in the array, there is no need for absolute measurements of the photodetector photocurrents. The output reading can be performed independently on the single interferometer waveguides and treated conveniently afterwards. While it is clear that the sensitivity of this reading method depends on the number of N-fold produced by the MMI splitter, this number cannot be increased indefinitely without compromising the overall robustness of the photonic structure. To overcome such a limitation, signal processing techniques of the output photocurrents can be employed, moving the complexity of the reading process to more traditional CMOS circuitry.

CONCLUSIONS

In this paper we propose a surface plasmon sensor based on an interferometer array that works in the visible range by using aluminium and amorphous silicon nitride for the core of the waveguide. We have investigated the decoupled plasmon modes on both sides of a waveguide interferometer using the FEM method and found good agreement between the predicted in phase and phase opposition distances and the transmitted maximum and minimum power using modal decomposition simulations. Furthermore, we have designed an MMI structure to excite 8 parallel waveguides each having a different interferometer length. The simulated output power of the array elements is dependent on the refractive index and we have observed that shifting of the minimum occurs as the refraction index increases. Interestingly, instead of scanning over the wavelength or the incident angle as usual, scanning over L offers an alternative as a possible interrogation scheme for Lab-On-Chip applications.

Acknowledgements: Research supported by EU funds through the FEDER European Regional Development Fund and by Portuguese national funds by FCT –Fundação para a Ciência e a Tecnologia with projects PTDC/NAN-OPT/31311/2017, UID/EEA/00066/2019, SFRH/BD/144833/2019, and by projects IPL/2019/BioPlas_ISEL and IPL/2019/MO-TFT_ISEL.

REFERENCES

[1] Chin, C. D., Linder, V. and Sia, S. K., “Lab-on-a-chip devices for global health: Past studies and future opportunities,” Lab Chip (2007).
[2] Dishman, E., Matthews, J. and Dunbar-jacob, J., [Everyday Health : Technology for Adaptive Aging] (2004).
[3] Nayak, S., Blumenfeld, N. R., Laksanasopin, T. and Sia, S. K., “Point-of-Care Diagnostics: Recent

Developments in a Connected Age," Anal. Chem. **89**(1), 102–123 (2017).
[4] Vashist, S. K., Luppa, P. B., Yeo, L. Y., Ozcan, A. and Luong, J. H. T., "Emerging Technologies for Next-Generation Point-of-Care Testing," Trends Biotechnol. (2015).
[5] Jason-Moller, L., Murphy, M. and Bruno, J., "Overview of Biacore Systems and Their Applications," Curr. Protoc. Protein Sci. (2006).
[6] Turner, A. P. F., "Biosensors: Sense and sensibility," Chem. Soc. Rev. (2013).
[7] González-Guerrero, A. B., Maldonado, J., Herranz, S. and Lechuga, L. M., "Trends in photonic lab-on-chip interferometric biosensors for point-of-care diagnostics," Anal. Methods (2016).
[8] Fantoni, A., Costa, J., Fernandes, M., Vygranenko, Y. and Vieira, M., "A simulation analysis for dimensioning of an amorphous silicon planar waveguide structure suitable to be used as a surface plasmon resonance biosensor," Proc. SPIE 11207, Fourth Int. Conf. Appl. Opt. Photonics, 112070A (2019).
[9] Debackere, P., Scheerlinck, S., Bienstman, P. and Baets, R., "Surface plasmon interferometer in silicon-on-insulator: Novel concept for an integrated biosensor," IEEE Int. Conf. Gr. IV Photonics GFP (2006).
[10] Wangüemert-Pérez, J. G., Hadij-ElHouati, A., Sánchez-Postigo, A., Leuermann, J., Xu, D. X., Cheben, P., Ortega-Moñux, A., Halir, R. and Molina-Fernández, Í., "Subwavelength structures for silicon photonics biosensing," Opt. Laser Technol. (2019).
[11] Rahim, A., Ryckeboer, E., Subramanian, A. Z., Clemmen, S., Kuyken, B., Dhakal, A., Raza, A., Hermans, A., Muneeb, M., Dhoore, S., Li, Y., Dave, U., Bienstman, P., Le Thomas, N., Roelkens, G., Van Thourhout, D., Helin, P., Severi, S., Rottenberg, X., et al., "Expanding the Silicon Photonics Portfolio with Silicon Nitride Photonic Integrated Circuits," J. Light. Technol. (2017).
[12] Porcel, M. A. G., Hinojosa, A., Jans, H., Stassen, A., Goyvaerts, J., Geuzebroek, D., Geiselmann, M., Dominguez, C. and Artundo, I., "Silicon nitride photonic integration for visible light applications," Opt. Laser Technol. (2019).
[13] Hu, J., Li, L., Lin, H., Zhang, P., Zhou, W. and Ma, Z., "Flexible integrated photonics: where materials, mechanics and optics meet [Invited]," Opt. Mater. Express (2013).
[14] Subramanian, A. Z., Neutens, P., Dhakal, A., Jansen, R., Claes, T., Rottenberg, X., Peyskens, F., Selvaraja, S., Helin, P., Dubois, B., Leyssens, K., Severi, S., Deshpande, P., Baets, R. and Van Dorpe, P., "Low-Loss Singlemode PECVD silicon nitride photonic wire waveguides for 532-900 nm wavelength window fabricated within a CMOS pilot line," IEEE Photonics J. (2013).
[15] Kageyama, S., Akagawa, M. and Fujiwara, H., "Dielectric function of a-Si:H based on local network structures," Phys. Rev. B - Condens. Matter Mater. Phys. **83**(19) (2011).
[16] Zeng, S., Baillargeat, D., Ho, H. P. and Yong, K. T., "Nanomaterials enhanced surface plasmon resonance for biological and chemical sensing applications," Chem. Soc. Rev. (2014).
[17] Costa, J., Fantoni, A., Lourenço, P. and Vieira, M., "Simulation of a parallel waveguide array structure suitable for interrogation scheme in a plasmonic biosensor," SPIE PHOTONICS WEST, Phys. Simul. Optoelectron. Devices XXVIII Pap. 11274-83 (2020).
[18] Homola, J., "Electromagnetic Theory of Surface Plasmons" (2006).
[19] Rakić, A. D., Djurišić, A. B., Elazar, J. M. and Majewski, M. L., "Optical properties of metallic films for vertical-cavity optoelectronic devices," Appl. Opt. (1998).
[20] Perez, A. M., Santiago, C., Carrillo, F. R. and Zuniga, C., "Optical properties of amorphous hydrogenated silicon nitride thin films," Opt. Eng. 45(12), 1–4 (2006).
[21] Lourenço, P., Fantoni, A., Costa, J. and Vieira, M., "Lithographic Mask Defects Analysis on an MMI 3 dB Splitter," Photonics **6**(4), 118 (2019).
[22] Soldano, L. B. and Pennings, E. C. M., "Optical Multi-Mode Interference Devices Based on Self-Imaging: Principles and Applications," J. Light. Technol. (1995).